Non-axisymmetric Flow Development in Pulsatile Blood Flow through an Aneurysm

R.A. Jamison[1,2], G.J. Sheard[1,2] & K. Ryan[1]

[1]Fluids Laboratory for Aeronautical and Industrial Research (FLAIR), Department of Mechanical Engineering, Monash University, VIC, 3800, Australia.

[2]Monash University Biomedical Engineering Technology Alliance (MuBeta), Monash University, VIC, 3800, Australia.

Abstract

Computational fluid dynamics modelling of an abdominal aortic aneurysm is commonly simplified to consider a two-dimensional axisymmetric problem. To determine the validity of this assumption, a Floquet stability analysis was employed to predict the conditions under which an axisymmetric aneurysmal flow is unstable to non-axisymmetric instabilities. Dimensions of the model were selected to be consistent with a high-risk aneurysm in the human abdominal aorta. In particular, the model consisted of an elliptical bulge defining the aneurysm, and both upstream and downstream artery sections. A sinusoidal time-varying parabolic velocity profile was input upstream, with Womersley number $\alpha = 16.9$ (representing a heart rate of 70 beats per minute when artery diameter $D = 22.7$ mm and kinematic viscosity $v = 3.3 \times 10^{-6}$ m^2/s). A Reynolds number range relevant to aneurysms in large arteries was examined, with the critical Reynolds number for non-axisymmetric transition and the corresponding azimuthal wavelength found to be $Re_{\mathrm{CRIT}} = 610$ and $\lambda = \pi$ (azimuthal mode number $m = 2$). The maximum vorticity at the vessel wall was found to occur at the distal end of the aneurysm bulge. The pulsatile flow frequency was also varied, with the frequency dependence on Re_{CRIT} and λ being established.

Keywords: Aneurysm, computational fluid dynamics, Floquet stability analysis, three-dimensional transition, non-axisymmetric flow.

Introduction

An aneurysm is a localised, blood-filled dilation of a blood vessel caused by disease or weakening of the vessel wall [19]. There are two main groups of aneurysm; fusiform and saccular [9]. Fusiform aneurysms are primarily found in the abdominal aorta and saccular aneurysms are most commonly found in the main arteries of the cerebral circulation. The shape of the two types differs greatly, as shown in Figure 1, with fusiform being a bulge along the length of the blood vessel, and saccular being a bulge from one side of the wall. This study investigates the most common fusiform aneurysm, the Abdominal Aortic Aneurysm (AAA), which is usually located upstream of a major abdominal bifurcations [9].

The formation of an aneurysm results from the deformation that occurs due to the pulsatile pressure over each cardiac cycle [20]. Degradation of the vessel wall tissue can occur over time; as the ratio of elastin to collagen decreases, the vessel progressively loses its elasticity [9]. When the vessel wall eventually becomes too weak, the aneurysm will rupture, which leads to death in almost 90% of cases [6], with AAA rupture being the 15th leading cause of death in the United States of America [18]. AAA rupture occurs when the stress within the aneurysm wall exceeds the tensile strength of the wall [20]. Prediction of the point at which rupture will occur requires the calculation of the tensile stress on the patients' aneurysm wall and the maximum stress before failure at that point [9], however measuring the tensile stress is very difficult, making prediction of rupture problematic.
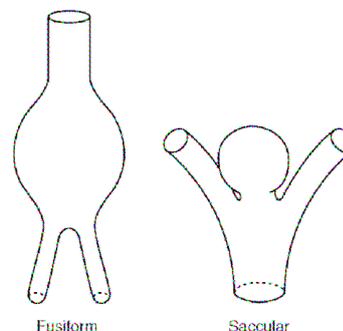
Figure 1: Classification of aneurysms based on shape [9]. Fusiform aneurysms (the focus of this study) are a bulge along the length of a blood vessel and Saccular aneurysms have a bulge from one side.

Today factors such as genetic disorders, mycotic infection, high blood pressure, effects of cigarette smoking, atherosclerosis, and aging have become prevalent [9]. Age is the most common factor in AAAs, with individuals under the age of 50 rarely having them. However, their incidence increases drastically by age 55, and peaks in the early 80s [9]. Abdominal Aortic Aneurysms (AAAs) are present in more than 3% of the general population, with 9% of men over the age of 60 having them, representing the most greatly affected demographic [18]. At present there is no reliable basis on which to evaluate susceptibility to rupture of a particular AAA. Medical intervention requires the risk of rupture to be weighed against operation morbidity [9]. Intervention is sought when the cumulative risk for rupture exceeds risk of surgery, within the context of overall life expectancy of the patient [5]. Surgical treatment is currently recommended for AAAs exceeding 5 cm in maximal diameter and those with expansion rates >0.5 cm/year [4]. This is concerning as some aneurysms grow steadily whereas others seem to grow rapidly, reach a certain size, and then suddenly slow their expansion rate [9], this unsteady growth can lead to unexpected rupture. Additionally these methods for determining the need for medical intervention do not take into account the precise geometry of the AAA, nor the fluid stresses acting on the aneurysm walls.

Previous research into this field has shown that pressures and stresses present in an aneurysm are highly dependant not only on the size, but also the shape and symmetry of the aneurysm, as found by Vorp *et al.* [21]. However, research into aneurysms using computational fluid dynamics commonly simplifies the

geometry and the symmetry of the flow to reduce the complexity of the modeled system. For example, Cowling *et al.* [5], Salsac *et al.* [13] and Sheard *et al.* (2007) [14] considered an axisymmetric geometry, with the numerical simulations of Sheard *et al.* (2007) [14] considering only axisymmetric flow. While Cowling *et al.* [5], Salsac *et al.* [13] and Lasheras [9] have observed possible flow asymmetry in axisymmetric fusiform aneurysms, no study has yet sought to investigate the onset of this non-axisymmetric flow. The present study investigates this using a non-axisymmetric Floquet stability analysis technique. Neglecting to take this three-dimensionality into account in previous studies may have limited the application of their findings. Thus an improved understanding of the stability and dynamics of blood flow through aneurysms is required to accurately predict the stresses present and their potential to cause rupture.

This study aims to determine if the axisymmetric assumption made by studies when computing aneurysmal flow is valid, by considering the stability of axisymmetric flow in a fusiform aneurysm model to non-axisymmetric perturbations. This is conducted under a range of Reynolds numbers and pulsatile flow conditions chosen to mimic conditions experienced by physical blood flows. This analysis will provide a prediction of the critical Reynolds number (Re_{CRIT}) for which the transition from axisymmetric to fully three-dimensional flow occurs, with the intention being to determine if future research into this axisymmetric assumption is required. Additionally, the growth rate and structure of three-dimensional instabilities present in the geometry was investigated, and the Reynolds number dependence and frequency dependence of these global instabilities was determined.

Methodology

The numerical investigation of idealised aneurysms usually uses several common geometric features to define the geometry. Figure 2 show the major dimensions of a common idealised axisymmetric geometry, where L is the bulge length, W is the bulge width, D is the undilated blood vessel diameter, U is the time-averaged mean flow velocity and R_c $(R_c = R / D)$ is the normalised radius of curvature between the blood vessel and the aneurysmal bulge.
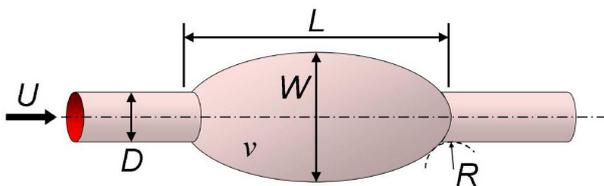
Figure 2: Common idealised aneurysm with major dimensions [14]; where L and W are the length and width of the aneurysm, D is the undilated blood vessel diameter, U is the time-averaged mean flow velocity and R is the radius of curvature.

The model geometry used in this study has been chosen to be representative of typical abdominal aortic aneurysms, with the geometry parameters of $L / D = 4$, $L / W = 1.76$, $R_c = 0.5$; the proximal (upstream) and distal (downstream) artery segments are each $3D$ in length. The inclusion of a radius of curvature between the blood vessel and the aneurysmal bulge, as opposed to a sharp edge, is used to give a more realistic interface. The proximal and distal artery segments are present to ensure accurate flow development through the aneurismal bulge. To remain consistent with previous research, the amplitude of the inlet velocity used is U/2 [14]. The periodic time history of blood flow is approximated using the sinusoidal function

$$\frac{u_{inlet}}{U} = \frac{u_{profile}}{U} \times (1 + \frac{1}{2}\sin(\omega t)) \ ,$$
$$\mathrm{v}_{inlet} = 0 \ ,$$
$$\mathrm{w}_{inlet} = 0 \ ,$$

where

$$u_{profile} = 8 \times (0.25 - y^2) .$$

This simplification is used in these simulations as a realistic heart beat produces periodic results, with the frequency of the heart rate forcing the flow to adopt its frequency [13]. It is also useful as heartbeat waveforms differ depending on the location within the body, so an approximate signal reduces the number of parameters adopted in this model, with Blackburn & Sherwin [3] seen to utilise a similar profile in their simulations. Figure 3 shows the function used and the points in the cardiac cycle (at the *inlet*) at which numerical values were calculated. Point c is representative of the peak systole, and point g the peak diastole.
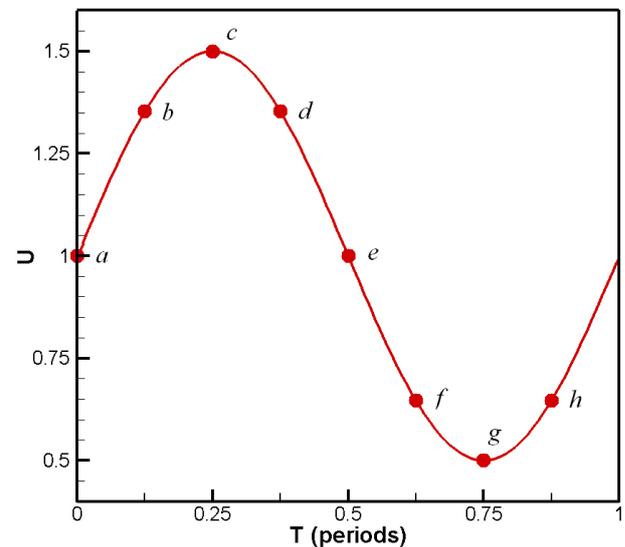
Figure 3: Sinusoidal approximation of heart beat used in this study. One period of u_{INLET} is displayed, with points a-h representing the time at which numerical values were calculated.

A parabolic profile is used for the inflow condition, which is a simplification of the true Womersley solution for periodic pipe flows. In practice, though, the flow is found to quickly adapt to a Womersley profile in the proximal artery segment. The parabolic assumption has been validated by Morris *et al.* [11] to have only a small effect on the difference in outlet flow rates for an idealized model (5%) when compared to a realistic pulsatile profile. The initial flow field throughout the domain is u_{inlet} applied along the central core of the geometry, with zero velocities in the outer region of the aneurysm bulge.

For pulsatile circulatory flow, two dimensionless parameters are typically used to characterise the flow conditions; the Reynolds number and the Womersley number. The Reynolds number is defined as

$$Re = \frac{UD}{\nu} \ ,$$

where ν is the kinematic viscosity (for whole blood $v \approx 3.3\mathrm{x}10^{-6}$ m^2/s [11]). The Reynolds number was varied from 100 to 2000, to account for the various sizes and locations of aneurysms. The large range of Reynolds numbers studied ensures that this

354

research will be relevant to aneurysms that occur in various parts of the human body. The Reynolds number range chosen corresponds to blood vessel ranging over approximately 1-22mm, which not only covers the human abdominal aorta (generally 15-20mm [6]), but also smaller blood vessels found elsewhere in the body. For arteries greater than 0.5mm in diameter, the non-Newtonian and multi-phase properties of blood can be safely ignored [8]. In these simulations blood is also assumed to be incompressible and homogeneous.

The second dimensionless parameter, the Womersley number, represents the ratio of unsteady force to viscous force, or the unsteady behaviour of fluid flow in response to an oscillatory pressure gradient [5]. The Womersley number is defined as

$$\alpha = \frac{D}{2}\sqrt{\frac{\omega}{\nu}} \, ,$$

where ω is the frequency of the pulsatile flow. Large Womersley numbers represent a pulsatile flow with large acceleration and deceleration [5]. The bulk of this study considers a constant Womersley number typical of resting heart conditions. For $\alpha = 16.9$ corresponds to a heart rate of 70 beats per minute if $D = 22.7$ mm and $\nu = 3.3 \times 10^{-6}$ m^2/s.

The numerical simulations in this study were performed using an in-house spectral element software package which solves the incompressible time-dependant Navier–Stokes equations [7, 15 and 16]. Within each element, polynomial shape functions are employed, and high spatial convergence is achieved by the use of efficient Gauss-Legendre-Lobatto quadrature. Spatial resolution can be controlled by varying the polynomial degree (N) within each element. A grid independence study was conducted in order to determine the mesh density required to obtain high accuracy whilst ensuring the computational expense did not exceed the restrictions of the given timeframe for this study. The highest Reynolds number investigated in this study ($Re = 2000$) was used as the test case as higher Reynolds number flows are more sensitive to resolution deficiencies in simulations. An L_2 norm of the velocity was taken periodically, with the period being equal to that of the inflow. The L_2 norm is the integral of the velocity magnitude over the domain, and is defined as

$$L_2 \text{ norm} = \int_{\Omega} |\mathbf{U}| \, d\Omega \, ,$$

where Ω is the computational domain and $|\mathbf{U}|$ is the velocity magnitude. Figure 4 shows the convergence of the solution to a periodic state for simulations employing element polynomial degrees N = [4–8]. The plot shows that a periodic solution is reached after approximately seven periods of the inflow.

The L_2 norm of each periodic flow was compared to the highest resolution case, providing an estimate of the percentage uncertainty of each case. These results are plotted in Figure 5 for element polynomial degree N = [4–9]. This concluded that for polynomials above degree 7, there was a negligible gain in accuracy. Hence elements of degree 7 were used hereafter.

The data obtained from the grid independence study was compared to the PIV measurements of Salsac *et al.* [13] to qualitatively validate the computed results. The two-dimensional vorticity of the computed flow (Figure 6*a*) was compared to the instantaneous vorticity measured by PIV (Figure 6*b*). The experimental setup employed different geometric parameters and inlet flow function to the present computations, but nevertheless

the CFD results were seen to produce the same general flow topology. Regions of vorticity develop at the proximal and distal ends of the aneurysms walls, with a thin negative zone of vorticity along the remainder of the aneurysmal wall. Also significant is a vortex ring propagating along the centre of the aneurysm, which forms due to the expansion at the upstream end of the aneurysm. The observed vortex ring in the computed flow is narrower than that in the PIV measurements, which may be due to the size difference of the models. Also, the limited resolution of the PIV measurements prevents a detailed comparison of the smaller scale structures to be made.
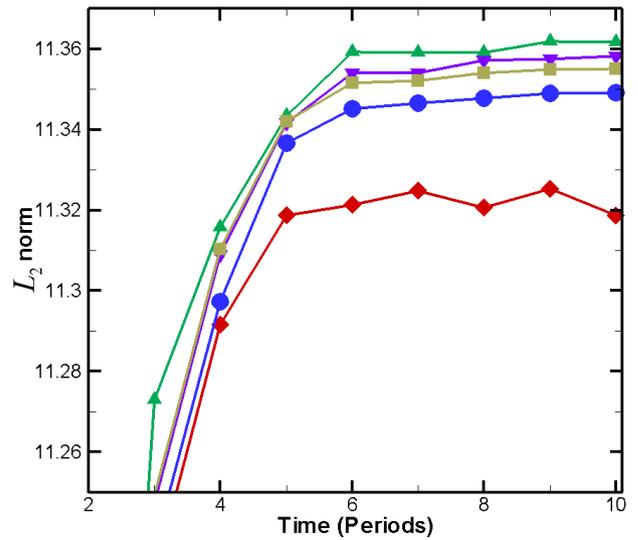
Figure 4: Convergence of the numeric solution at $Re = 2000$ for various values of polynomial degree N. L_2 norm calculated at point b, just before peak systole. Diamonds represent N = 4, deltas N = 5, circles N = 6, gradients N = 7 and squares N = 8.
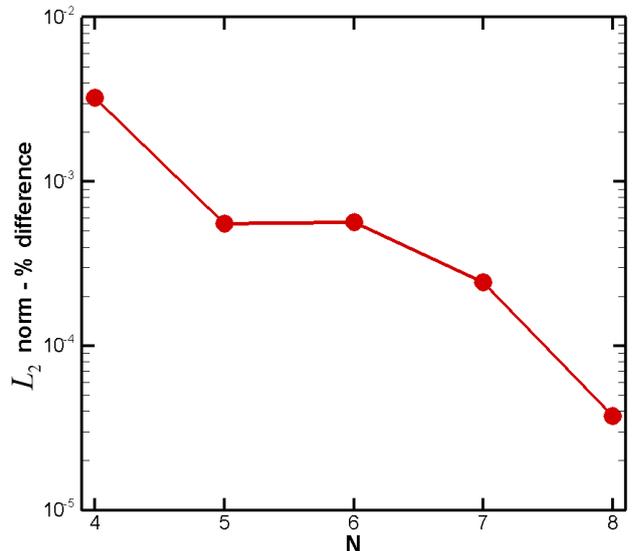
Figure 5: Percentage difference in L_2 norm of the velocity against element polynomial degree N. Simulations conducted with $Re = 2000$ and $\alpha = 16.9$.

In order to determine if three-dimensional features are present in the flow, a linear stability analysis technique is used. Floquet stability analysis provides a prediction of the three-dimensional instabilities in a steady or periodic axisymmetric flow [1, 16 and 17]. This is achieved by inspecting the evolution of a small three-dimensional perturbation to a two-dimensional base flow. Floquet analysis returns an eigenvalue representing the magnitude of the Floquet multiplier |μ|, which in turn represents an amplification factor applied to the three-dimensional

perturbation between successive periods. If $|\mu| \geq 1$, the perturbation will grow over time and the solution is considered unstable. If $|\mu| < 1$, the perturbation will decay and the axisymmetric flow is stable. The perturbations are periodic in the azimuthal direction, with azimuthal wavelength $\lambda = 2\pi / m$, where m is the mode number. The perturbation fields are solved using the linearised Navier-Stokes equations, which decouples each individual azimuthal mode of the three-dimensional perturbation. This permits us to analyse the stability of individual wavelengths in isolation, thus greatly reducing the computational expense.
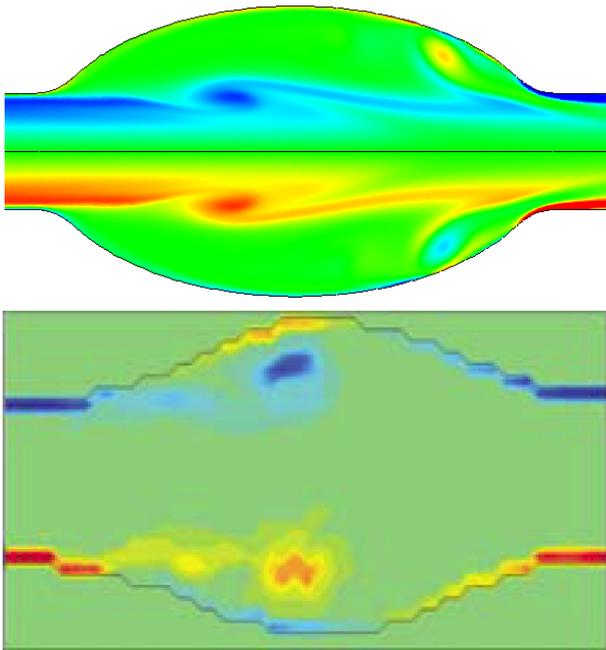
Figure 6: Vorticity measurements taken just after peak systole occurred at the inlet of the model. *a*: Vorticity of computational simulation *b*: Instantaneous vorticity measured using PIV conducted by Salsac *et al.* [13] ($L / D = 2.9$ and $L / W = 1.38$)

Several azimuthal wavelengths were investigated in order to determine the wavelength that would dominate the three-dimensional characteristics of the flow. However, axisymmetry imposes a restriction whereby only integer modes are available. The first four modes will be investigated, representing wavelengths of 2π, π, $2\pi/3$ and $\pi/2$, as studies have shown that these modes are consistently more unstable than higher mode numbers [13,14], which are inevitably damped by viscous effects. Investigation of the next four modes (mode numbers $5 - 8$) was conducted for higher Reynolds numbers to determine the dominant wavelength for each Reynolds number investigated.

For the chosen range of Reynolds numbers the base flow field simulations were evolved until a periodic solution was reached. The verification of periodicity was once again conducted by inspecting the L_2 norm of the flow. The Floquet stability analysis was then applied to the base flow fields for the chosen stability wavelengths.

Results

Figure 7 presents the Floquet multiplier in terms of the azimuthal wavelength for the idealised axisymmetric geometry investigated, for $Re = [500, 750]$. Examination of Figure 7 enables the determination of both the Reynolds number and the azimuthal wavelength for which transition to three-dimensional flow will occur. The critical Reynolds number was found to be

$Re_{CRIT} = 610$, with the transition occurring at mode number $m = 2$, corresponding to an azimuthal wavelength of $\lambda = \pi$. This result was unexpected as it is usually the larger wavelength of mode number $m = 1$ (2π) that is most unstable for axisymmetric flows [10,2,16].

Figure 8 displays the Floquet Multiplier in terms of azimuthal wavelength, with modes numbers $1 - 4$ plotted for $Re = [100,1000]$. Inspection of Figure 8 enables a prediction of which mode will dominate the three-dimensionality in the flow for a range of Reynolds numbers. A clear trend was observed between the Reynolds number and the dominant wavelength. As the Reynolds number was increased, the wavelength that dominated the three-dimensional flow was found to decrease. For Reynolds numbers above Re_{CRIT} the dominant modes were mode number $m = 2$ from $610 \leq Re \leq 750$ and mode number $m = 3$ from $750 < Re \leq 1000$. However, for $Re > Re_{CRIT}$ the solutions may not provide an accurate prediction of the flow.
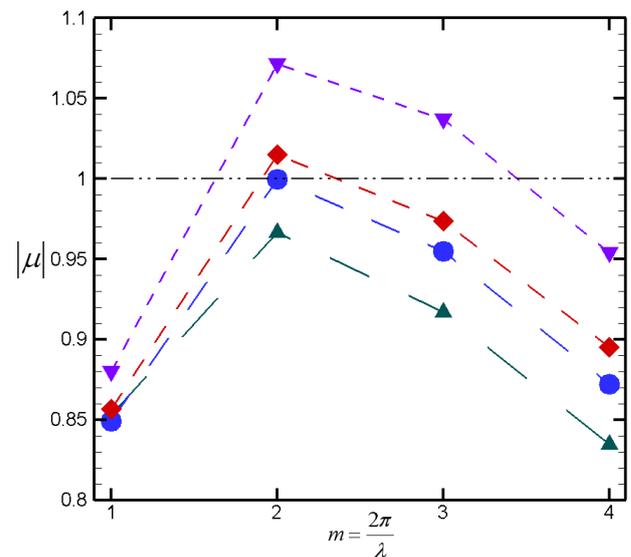
Figure 7: Floquet multiplier plotted against mode number m for $Re = [500, 750]$. The dash-dot line represents the stability threshold. Deltas represent $Re = 500$, circles $Re = 610$, diamonds $Re = 650$ and gradients $Re = 750$.
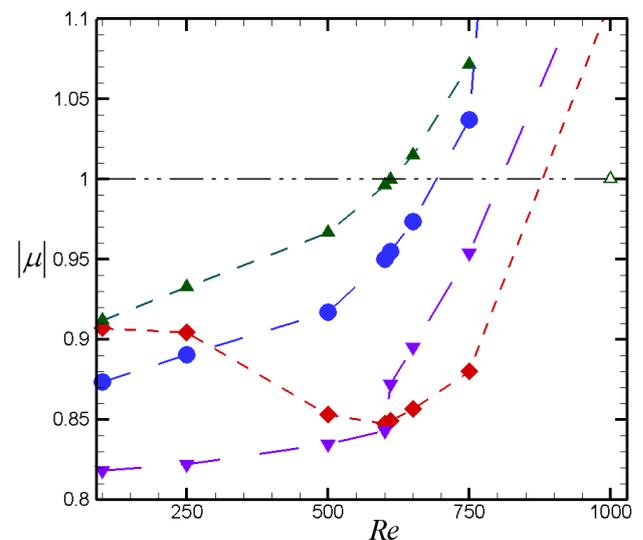
Figure 8: Floquet multiplier plotted against Re for mode numbers $m = [1, 4]$. The dash-dot line represents the stability threshold. Diamonds represent $m = 1$, deltas $m = 2$, circles $m = 3$ and gradients $m = 4$. Filled symbols represent regular Floquet multipliers whereas hollow symbols represent incommensurate Floquet multipliers.

356
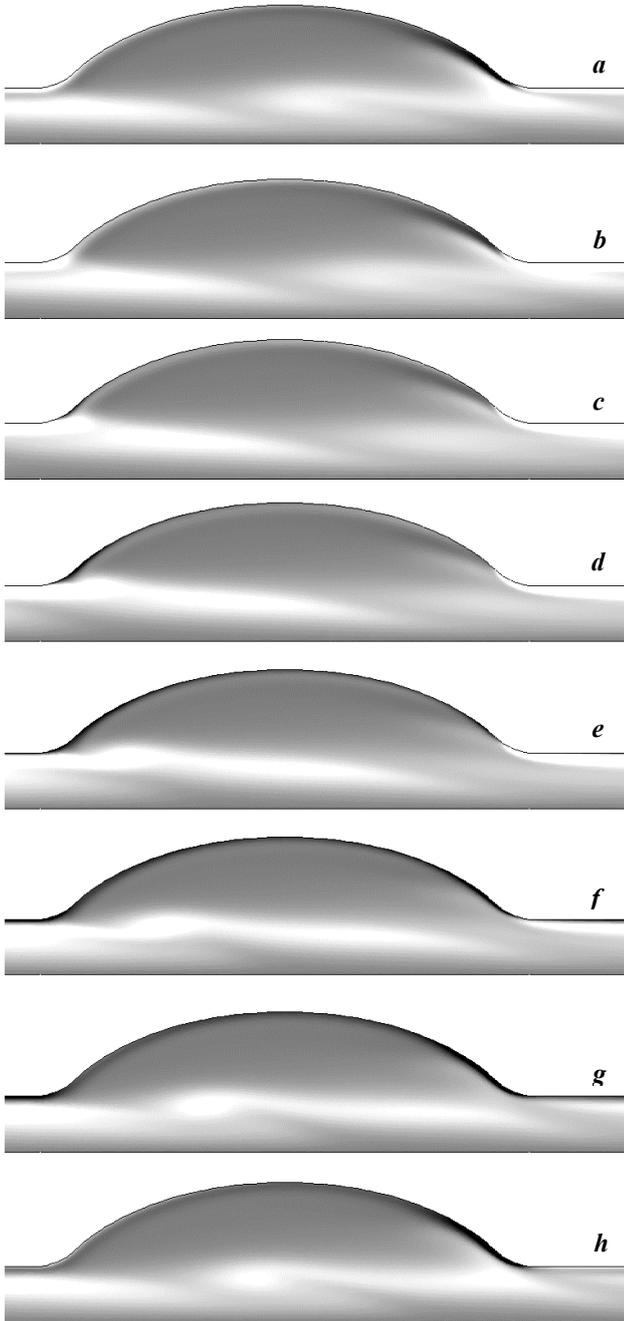
Figure 9: Vorticity contours for the base flow with $Re = Re_{CRIT}$. Each figure represents a snapshot of the base flow development each taken at 1/8 period progression. The bottom boundary is an axis of symmetry. Black represents negative vorticity and white represents positive vorticity.
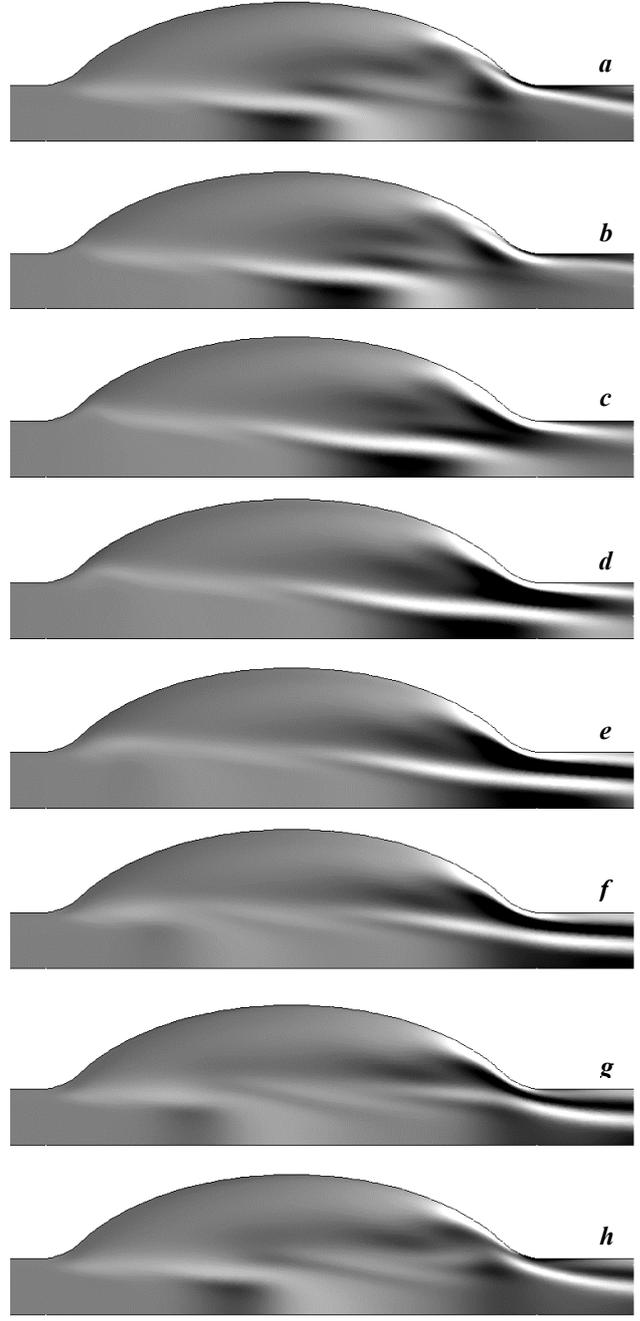
Figure 10: Streamwise perturbation vorticity contours for mode number $m = 2$ with $Re = Re_{CRIT}$. Each figure represents a snapshot of the mode development each taken at 1/8 period progression. The bottom boundary is an axis of symmetry for the base flow. Black represents negative vorticity and white represents positive vorticity.
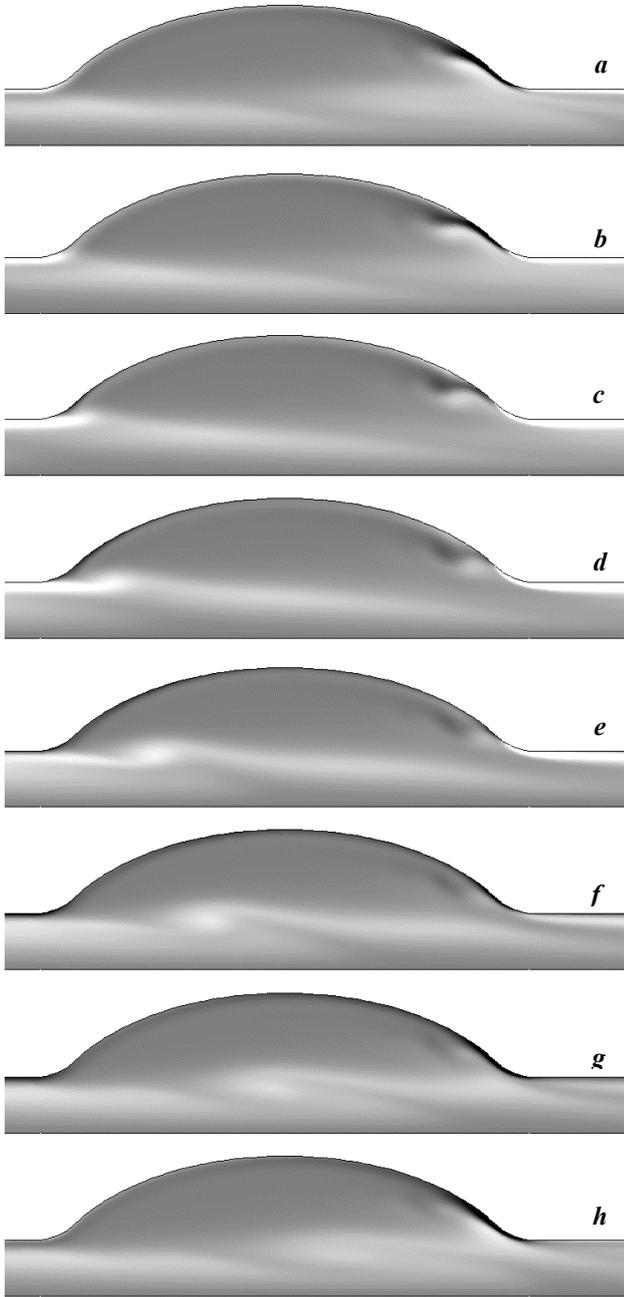
Figure 11: Vorticity contours for the base flow with *Re = 750*. Each figure represents a snapshot of the base flow development each taken at 1/8 period progression. The bottom boundary is an axis of symmetry. Black represents negative vorticity and white represents positive vorticity.
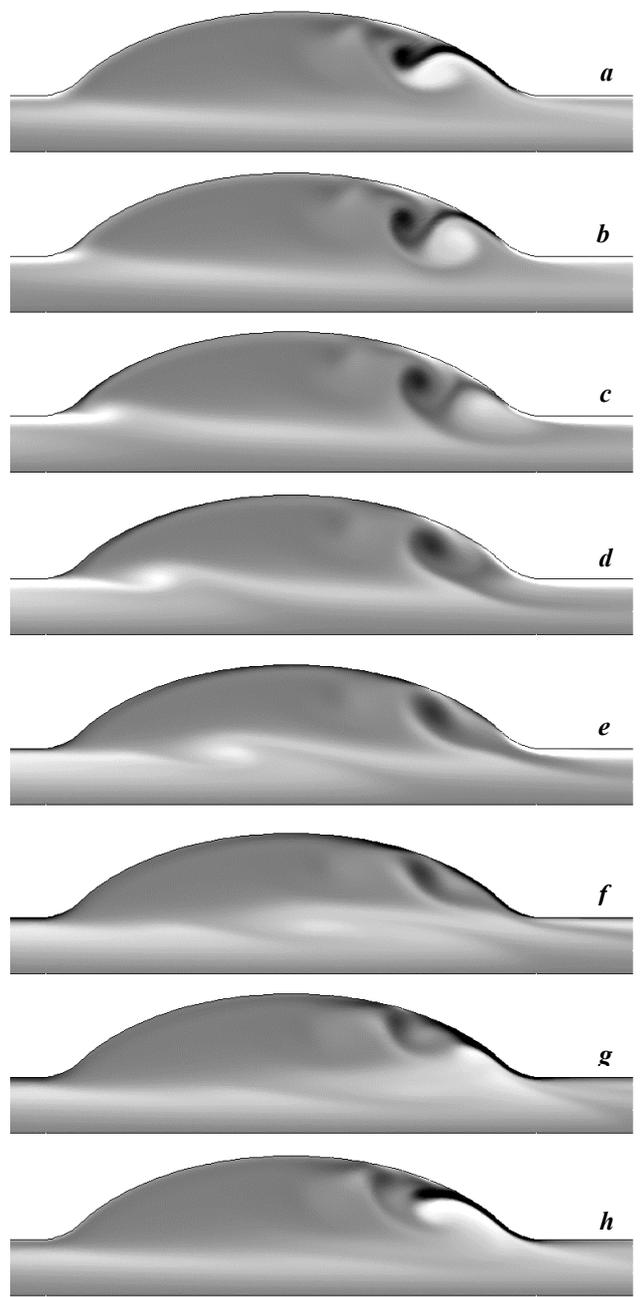
Figure 12: Vorticity contours for the base flow with *Re = 1000*. Each figure represents a snapshot of the base flow development each taken at 1/8 period progression. The bottom boundary is an axis of symmetry. Black represents negative vorticity and white represents positive vorticity.

Figures 9 and 10 display the base flow vorticity field and the streamwise perturbation vorticity field, respectively, for the dominant mode number ($m = 2$) at $Re = Re_{CRIT}$ for a complete cardiac cycle with a 1/8 period progression. Labeling of the position in the cardiac cycle that each image obtained is as per Figure 3.

The base flow vorticity in Figure 9 displays two main regions of vorticity. The first is seen most clearly in Figure 9c at the beginning of the distal artery segment at the wall as the peak diastole passes to the distal artery segment. The second region is the vortex ring that propagates along the centre of the aneurysm (Figure 9e – h). However, this vortex ring in the base flow is seen to have little effect on in the $m = 2$ perturbation vorticity field (Figure 10e – h). The vorticity is seen to vary substantially over each cardiac cycle, though the peak vorticity of the $m = 2$ instability is consistently found to occur at the distal end of the aneurismal bulge at the vessel wall. As the peak diastole progresses from the aneurysm to the distal artery segment (Figure 10d – e) the strength of the perturbation vorticity is seen to grow as a function of time. Following this, the peak systole passes from the proximal artery segment to the aneurismal bulge and the flow separates, creating a vortex in the base flow just above the central flow (Figure 9f). This initial vortex creates the large recirculation region that occurs in the aneurismal bulge and as peak systole eventually passes from the aneurysm to the distal artery segment (Figure 10h-a), the peak vorticity structure for mode number $m = 2$ is seen to decrease in size.

A region of negative vorticity is also seen to form below this peak vorticity area just after the peak diastole moves from the aneurismal bulge to the distal artery segment (Figure 10d – e). As this negative vortex occurs away from the vessel wall in the distal segment of the blood vessel the velocity at this point is heavily dependant on the position in the cardiac cycle, and thus so is the vorticity. As the cardiac cycle progresses and the peak systole moves to the end of the aneurismal bulge (Figure 10h – a) the negative vortex has little influence on the stability of the flow.

The stability analysis conducted at $Re > 750$ produced several non-converging Floquet multipliers. There are three types of modes that can arise in a Floquet stability analysis; which differ in how μ bifurcates through the unit circle; a regular mode, a sub-harmonic mode and a quasi-periodic mode. A regular mode has only a positive real component of μ, a sub-harmonic mode has only a negative real component, and a quasi-periodic mode has an imaginary component [2]. The magnitude of the Floquet multiplies for the quasi-periodic modes identified in this study were evaluated as the mean of the estimates of |μ| acquired over many periods once the leading mode had been isolated. All the quasi-periodic modes found displayed subharmonic characteristics, indicating that the real component of the complex pair was negative. In each case investigated these quasi-periodic modes were never the dominant mode, and thus their effects would not be seen in the actual three-dimensional flow. Notably these quasi-periodic modes were only present for Reynolds numbers greater than Re_{CRIT}. One theory is that these modes are a result of the change in the axisymmetric base flow that is seen to occur between a Reynolds number of 750 and 1000. This transition in the structure of the base flow is displayed for a complete cardiac cycle with 1/8th period intervals in figures 11 and 12. It is in this Reynolds number range that the flow begins to change and develop a strong primary vortex (Figure 12a) as compared to the relatively weak recirculation that occurs at lower Reynolds numbers (Figure 11a). This primary vortex forms as peak systole leaves the aneurismal bulge and continues into the distal artery segment, causing a large separation in the flow. However, even as there is a link between incommensurate modes

occurring and the presence of the primary vortex, regular modes were still observed at these higher Reynolds numbers.

Figure 13 shows the Floquet multiplier in terms of the azimuthal wavelength with $Re = 750$ for α = [12, 25.2]. As α is increased (representing increasing the heart rate) smaller Floquet multipliers are produced. Thus we can conclude that when investigating higher heart rates the Reynolds number range for which flow will be axisymmetric will be greater than that for lower heart rates. A notable feature of Figure 13 is that at α = 12 and α = 15, characteristics are observer which are not found at the higher Womersley numbers investigated. It is in the Womersley number range from 15 - 16.9 that the structure of the flow makes an analogous transition to that witnessed in the Reynolds number range of 750 - 1000. Once again, the base flow begins to develop a strong primary vortex at the distal end of the aneurysm after peak systole. Notably, only heart rates that displayed the primary vortex returned quasi-periodic modes.
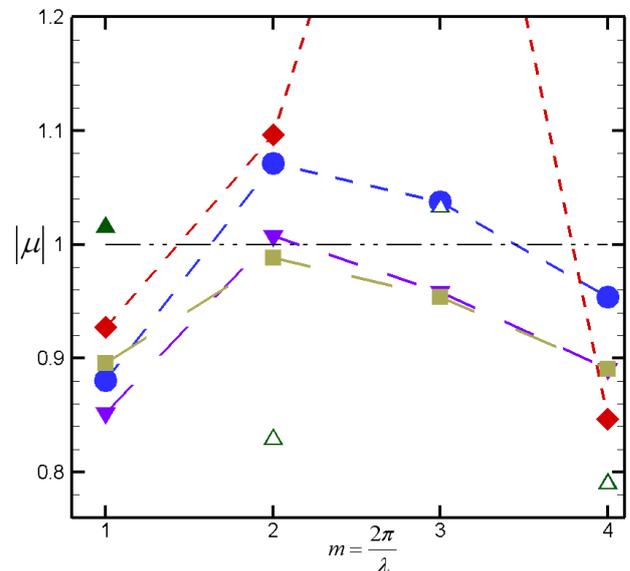
Figure 13: Floquet multiplier plotted against mode number m for $Re = [12, 23.6]$. The dash-dot line represents the stability threshold. Diamonds represent α = 12.0, deltas α = 15.0, circles α = 16.9, gradients α = 19.8 and squares α = 23.6. Filled symbols represent regular Floquet multipliers whereas hollow symbols represent incommensurate Floquet multipliers.

Discussion

The calculation of the critical Reynolds number for which three-dimensional flow will occur allows a determination of the diameters of blood vessels for which axisymmetric simulations are appropriate. It is predicted that for $Re < 610$ the flow will be axisymmetric for this particular geometry. This has an important bearing on studies of Abdominal Aortic Aneurysms, and requires more attention. With these aneurysms occurring in blood vessel diameters ranging from 15-20mm (relating to a Reynolds number range of 1300 – 1800), previous research may not have provided an accurate representation of the flow characteristics that are present in an AAA. Further research is required to determine exactly how the observed three-dimensionality will effect the findings of previous investigations that have used this axisymmetric assumption. This will require fully three-dimensional simulations to determine the actual wall shear stresses and pressure gradients present in an axisymmetric domain so a comparison can be made to results gained using the axisymmetric assumption. Other geometric ratios will also need to be investigated to determine the effect of geometry on the

transition to three-dimensional flow. A second consideration that needs to be taken into account is the Womersley number that is being investigated. If a low Womersley numbers are being considered, the range of Reynolds numbers available to be investigated will be reduced as non-axisymmetric flow will develop at a lower Reynolds number.

An investigation of $Re = Re_{CRIT}$ for other geometries will establish the sensitivity of the three-dimensionality to the various geometric parameters, so as to allow a more focused investigation of the parameters that have the greatest effect. The occurrence of the maximum vorticity at the vessel wall in the distal region of the aneurysmal bulge infers that Re_{CRIT} may be sensitive to the radius of curvature used in the geometry studied. In physical terms this means that the shape of the aneurysm at the distal end of the aneurysm could play an important role in determining the extent of three-dimensionality in the flow.

Conclusions

This study has predicted the critical Reynolds number for the transition to three-dimensional flow to be 610 for an idealised axisymmetric aneurysm with $L/D = 4$, $L/W = 1.76$ and $R_c = 0.5$. The transition to three-dimensional flow was found to occur with $m = 2$, though beyond the onset of this transition, the flow stability was dominated by the higher modes numbers. The maximum perturbation fields were strongest at the distal end of the aneurysmal bulge, suggesting that non-axisymmetric structures would develop in this region. A strong correlation has been found between inflow frequency and the critical Reynolds number, with an increase of the inflow frequency resulting in a decrease of the critical Reynolds number.

The primary vortex was only observed in axisymmetric flows which were predicted to be unstable to three-dimensional perturbations, suggesting that this vortex may play a role in the development of three-dimensional instability in these flows. Consideration of the stability of an isolated vortex ring of similar circulation may be useful in determining the mechanism for non-axisymmetric flow development in aneurysmal flows.

Acknowledgements

References

[1] Barkley, D. & Henderson, R. D. 1996 Three-dimensional floquet stability analysis of the wake of a circular cylinder. Journal of Fluid Mechanics 322, 215–241.

[2] Blackburn HM & Lopez JM, On three-dimensional quasi-periodic Floquet instabilities of two-dimensional bluff body wakes, (2003) *Phys Fluids* 15(8): L57–60

[3] Blackburn HM & Sherwin SJ, Instability modes and transition of pulsatile stenotic flow: pulse-period dependence, (2007) *J Fluid Mech* 573: 57–88

[4] Brown PM, Zelt DT, Sobolev B. 2003. *The risk of rupture in untreated aneurysms: The impact of size, gender, and expansion rate*. J. Vasc. Surg. 37:280–84

[5] Cowling R., Soria J., *Flow Visualisation through Model Abdominal Aortic Aneurysm*, Fourth Australian Conference on Laser Diagnostics in Fluid Mechanics and Combustion The University of Adelaide, South Australia, Australia, 7-9 December 2005, 33-36

[6] Egelhoff CJ, Budwig RS, Elger DF, Khraishi TA. *Model studies of the flow in abdominal aortic aneurysms during resting and exercise conditions*. J Biomech 1999;32:1319–29.

[7] Karniadakis, E. & Triantafyllou, G.S. 1989 Frequency selection and asymptotic states in laminar wakes. J. *Fluid* Mech. 199, 441-469.

[8] Ku, D.N., 1997, "Blood flow in arteries", Annual review of Fluid Mechanics, 29, pp. 399-434.

[9] Lasheras J, 2007, *The Biomechanics of Arterial Aneurysms*, Annual Review of Fluid Mechanics, 39, 293-319

[10] Leweke, T. & Provansal, M. 1995 The flow behind rings - bluff-body wakes without end effects. J. *Fluid* Mech. 288, 265-310.

[11] Morris L. et al, *Effects of flat, parabolic and realistic steady flow inlet profiles on idealised and realistic stent graft fits through Abdominal Aortic Aneurysms (AAA)*, Medical Engineering & Physics 28 (2006), 19–26

[12] Natarajan, R., Acrivos, A., The instability of the steady flow past spheres and disks. *J. Fluid Mech.* 254 (1993), pp. 323–344

[13] Salsac A. et al, *Evolution of the wall shear stresses during the progressive enlargement of symmetric abdominal aortic aneurysms*, Journal of Fluid Mechanics (2006), 560, pp. 19-51

[14] Sheard, G.J., Evans, R.G., Denton, K.M. & Hourigan, K., Undesirable Haemodynamics in Aneurysms, In *Proceedings of the IUTAM Symposium on Unsteady Separated Flows and Their Control,* Hotel Corfu Chandris, Corfu, Greece, 18-22 June 2007

[15] Sheard, G.J., Leweke, T., Thompson, M.C. & Hourigan, K., Flow around an impulsively arrested circular cylinder, *Physics of Fluids*, 19(8), 083601, 2007.

[16] Sheard, G.J. & Ryan, K., Pressure-driven flow past spheres moving in a circular tube, *Journal of Fluid Mechanics (In Press)*, 2007

[17] Sheard, G.J., Thompson, M.C. & Hourigan, K., From spheres to circular cylinders: The stability and flow structures of bluff ring wakes, *Journal of Fluid Mechanics*, 492, 147-180, 2003.

[18] Singh K., Bonaa K.H., Jacobsen B.K., Bjork L., Solberg S., 2001, *Prevalence of and risk factors for abdominal aortic aneurysms in a population-based study* – The Tromso Study";American Journal of Epidemiology, 154, 236 –244.

[19] Stedman, 2002, *The American Heritage® Stedman's Medical Dictionary*, Houghton Mifflin Company, Massachusetts

[20] Steinman et al, 2003, *Computational modelling of arterial biomechanics: Insights into pathogenesis and treatment of vascular disease*, Journal of Vascular Surgery, 37, 5, 1118-1128

[21] Vorp DA, Raghavan ML, Webster MW. Stress distribution in abdominal aortic aneurysm: influence of diameter and asymmetry. J Vasc Surg 1998;27:632-9.